

High temperature thermal properties of thin tantalum nitride films

Elah Bozorg-Grayeli, Zijian Li, Mehdi Asheghi, Gil Delgado, Alexander Pokrovsky et al.

Citation: *Appl. Phys. Lett.* **99**, 261906 (2011); doi: 10.1063/1.3672098

View online: <http://dx.doi.org/10.1063/1.3672098>

View Table of Contents: <http://apl.aip.org/resource/1/APPLAB/v99/i26>

Published by the [American Institute of Physics](#).

Related Articles

Effects of heat treatment and contact resistance on the thermal conductivity of individual multiwalled carbon nanotubes using a Wollaston wire thermal probe

J. Appl. Phys. **111**, 054321 (2012)

A 3-dimensional time-resolved photothermal deflection “Mirage” method

Appl. Phys. Lett. **100**, 091908 (2012)

Thermal characterization of composites made up of magnetically aligned carbonyl iron particles in a polyester resin matrix

J. Appl. Phys. **111**, 054906 (2012)

How does folding modulate thermal conductivity of graphene?

Appl. Phys. Lett. **100**, 093107 (2012)

Thermal conductivity of solid monohydroxyl alcohols in polyamorphous states

Low Temp. Phys. **38**, 74 (2012)

Additional information on *Appl. Phys. Lett.*

Journal Homepage: <http://apl.aip.org/>

Journal Information: http://apl.aip.org/about/about_the_journal

Top downloads: http://apl.aip.org/features/most_downloaded

Information for Authors: <http://apl.aip.org/authors>

ADVERTISEMENT

NEW!

iPeerReview
AIP's Newest App



**Authors...
Reviewers...
Check the status of
submitted papers remotely!**

AIP | Publishing

High temperature thermal properties of thin tantalum nitride films

Elah Bozorg-Grayeli,^{1,a)} Zijian Li,¹ Mehdi Asheghi,¹ Gil Delgado,² Alexander Pokrovsky,² Matthew Panzer,² Daniel Wack,² and Kenneth E. Goodson¹

¹Department of Mechanical Engineering, Stanford University, Stanford, California 94305, USA

²KLA-Tencor Corporation, Milpitas, California 95035, USA

(Received 21 November 2011; accepted 4 December 2011; published online 29 December 2011)

Tantalum Nitride (TaN) films carry high heat fluxes in a variety of applications including diffusion barriers in magnetoresistive random access memory and buffer/absorbers in extreme ultraviolet masks. The thicknesses of these films are usually of the same order as the thermal energy carrier mean free path, which complicates the study of heat conduction. This paper presents thermal (cross-plane) and electrical (in-plane) conductivity measurements on TaN films with thicknesses of 50, 75, and 100 nm. Picosecond thermoreflectance is used to extract the thermal boundary resistance between TaN and Al and the intrinsic thermal conductivity of TaN for temperatures of 300–700 K. The data and the relative importance of boundary resistances, electron-boundary scattering, and electron-defect scattering are interpreted using the electrical and thermal transport data. These data facilitate comparison of the phonon and electron contributions to thermal conduction in TaN. © 2011 American Institute of Physics. [doi:10.1063/1.3672098]

Tantalum Nitride (TaN) is common as a diffusion barrier film in magnetoresistive random access memory.^{1–3} Such diffusion barrier films are essential for preventing intermixing between thin functional films. Recently, TaN has become the preferred absorber material for EUV masks. This absorber layer rests on a Ruthenium-capped Mo-Si material that forms the resonant reflector for EUV light. Both magnetoresistance random access memory and EUV mask applications involve high heat flux densities within the TaN layer and surrounding materials. Accurate thermal property data are therefore needed for thermal simulation of devices using this material to ensure they do not succumb to heat-related damage. Although the electrical properties of TaN are well cataloged,¹ there are few data in the literature on its thermal properties and essentially no data for the thermal conductivity of thin films.

This work presents cross-plane electrical conductivity and picosecond time-domain thermoreflectance (TDTR) measurements on TaN films from 50 to 100 nm in thickness (Fig. 1). Using the in-plane electrical conductivity data, we estimate the electron contribution to TaN thermal conductivity. Combining this result with the minimum phonon thermal conductivity of TaN offers an estimate of total in-plane thermal conductivity. The TDTR data includes the thermal boundary resistance (TBR) between Al and TaN ($R_{\text{Al-TaN}}$) and the out-of-plane intrinsic thermal conductivity (k_{TaN}). We compare the measured k_{TaN} with the in-plane k_{TaN} estimate obtained from electrical measurements and minimum phonon thermal conductivity theory (Fig. 1).

High-temperature TDTR measurements extract the TaN intrinsic thermal conductivity, as well as the Al-TaN TBRs. During these measurements, the samples remain housed in an optical access oven pumped to vacuum. Temperature ramps are in 100 K increments, with a 15 min hold at each level before measurement. The TDTR system utilizes a pas-

sively modelocked, 1064 nm, Nd:YVO₄ laser with a 9.2 ps pulsewidth and 82 MHz repetition rate.⁴ A beamsplitter separates the pulse into two components: pump and probe. The frequency-doubled pump beam, modulated at a frequency of 5 MHz, travels along a fixed path toward the sample. A linear delay stage controls the path length of the probe beam, managing the temporal offset between the pump and probe pulses. The probe pulse interrogates the change in reflectivity of a 50 nm Al transducer, deposited on top of the TaN samples, as a function of time after the pump pulse. Since the reflectivity of the top metal film changes linearly with temperature for small temperature rises, the system obtains an accurate measurement of the normalized temperature decay of the Al transducer through the underlying materials.⁵

In determining k_{TaN} using the principle of thickness dependent thermal resistance with samples of varying thickness, we usually assume the intrinsic film thermal conductivity does not vary between samples. This analysis neglects any potential reductions in thermal conductivity due to size effects in the film. These effects can include increased scattering rates on film boundaries or on regions of higher imperfection density. Since the mean free path (MFP) of electrons in TaN can be ~25 nm, such scattering effects may complicate calculation of

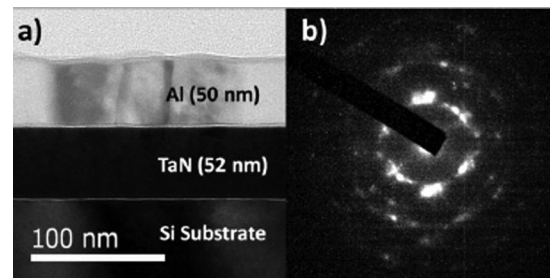


FIG. 1. (a) Cross-sectional TEM of Al on TaN on Si. The targeted TaN thickness is 50 nm. (b) Nanobeam diffraction shows the structure to be a mix of polycrystalline and amorphous TaN. The diffraction patterns are similar for all three thicknesses of TaN, implying that average grain size is not thickness dependent at this scale.

^{a)}Electronic mail: ebozorgg@stanford.edu.

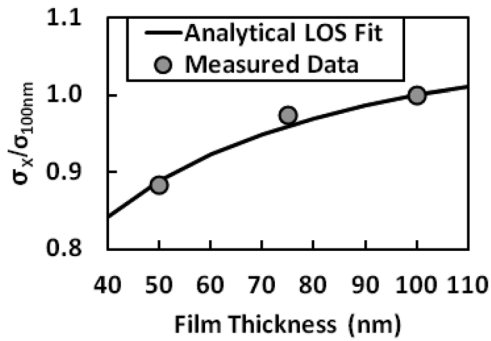


FIG. 2. Plot of electrical conductivity ratios between the 50, 75, and 100 nm TaN thin films. These ratios, in combination with Eq. (1), predict electron MFP. The above plot shows the best fit result ($\lambda_e = 30$ nm).

the cross-plane thermal conductivity of our films.¹ Primarily, the intrinsic thermal conductivity of the 50 nm film may be lower than that of the 100 nm film due to such effects. As a result, the thickness-independent solution may lead to inaccuracies in the out-of-plane k_{TaN} . It is therefore critical to determine how size effects modify the thermal behavior of these films.

In order to account for size effects in electron thermal conduction, we performed sheet resistance measurements of the 50 to 100 nm films. These measurements demonstrate thickness-dependence in the lateral electrical conductivity (σ_{lat}) of the film (Fig. 2). Using line of sight analysis, we extract, absent of boundary scattering effects and assuming similar morphology for all samples, the average electron MFP. For a medium with completely diffuse interfaces, this relation becomes⁶

$$\frac{\sigma_{\text{lat}}}{\sigma_{\text{bulk}}} = 1 - \frac{3}{2\delta} \int_1^\infty \left(\frac{1}{\xi^3} - \frac{1}{\xi^5} \right) (1 - \exp(-\delta\xi)) d\xi, \quad (1)$$

where σ_{bulk} is bulk TaN electrical conductivity assuming the same morphology as the thin films and δ is the ratio of film thickness, d , to bulk electron MFP, λ_e . Fitting Eq. (1) to the measured thickness dependent in-plane electrical conductivity for δ yields a bulk electron MFP of 30 nm (Fig. 2). Using a simple Matthiessen's rule approach ($\frac{1}{\delta} = \frac{1}{\lambda_e} + \frac{1}{d}$), this result indicates that the cross-plane electron thermal conductivity of the 50 nm film (given by $k_e = \frac{1}{3}C_e v_f \lambda$, where C_e is the volumetric electron heat capacity and v_f is the Fermi velocity) may be 20% less than that of the 100 nm film. Since the measurement temperatures are greater than half the Debye temperature of TaN,⁷ the Wiedemann-Franz-Lorenz law provides a reasonable estimate of the electron thermal conductivity. This value ranges from 2.8 to 3.1 $\text{W m}^{-1} \text{K}^{-1}$ for the 50-100 nm samples.

Since the TaN microstructure consists of a mixture of both crystalline and amorphous phases,⁸ minimum thermal conductivity theory offers a practical estimate of phonon thermal conductivity ($k_{p,\text{min}}$).⁹ In this analysis, we assign the carrier MFP to be equal to interatomic spacing in TaN. The relation, $k_{p,\text{min}} = \frac{1}{3}C_p v_p \lambda_p$ (where C_p is the volumetric heat capacity,¹⁰ v_p is the average phonon velocity,¹⁰ and λ_p is the average phonon MFP calculated from TaN density¹⁰), gives the minimum phonon thermal conductivity. This gives $k_{p,\text{min}} \sim 1.4 \text{ W m}^{-1} \text{K}^{-1}$ at 300 K. By summing the contribu-

tions from both electrons and phonons and assuming isotropic conduction, we estimate the intrinsic thermal cross-plane conductivity of TaN at room temperature to be $\sim 4.0\text{--}4.3 \text{ W m}^{-1} \text{K}^{-1}$ for the 50-100 nm films.

In order to extract k_{TaN} from our TDTR measurements, we solve the radially symmetric heat diffusion equation for conduction through the material stack and fit the solution to the experimental thermal response data.^{11,12} Since the measurement for each individual film is only sensitive to the lumped thermal resistance of the TaN layer and $R_{\text{TaN-Si}}$, we separate the TaN volumetric resistance from $R_{\text{TaN-Si}}$ by simultaneously fitting the thermal properties of all three samples to extract an accurate measure of the out-of-plane k_{TaN} . Since the pump and probe beams in this technique are roughly 100 times wider than the thickness of the TaN films, the measurement is insensitive to the in-plane k_{TaN} . Although it is valid to assume that the TBRs are constant for all three samples at each temperature, we have shown that the same assumption is not true for k_{TaN} . We can account for the size effect by modeling k_{TaN} as a combination of minimum phonon conductivity and thickness-dependent electron thermal conductivity

$$k_{\text{TaN}}(d) = k_{p,\text{min}} + \frac{1}{3}C_e v_f \left(\frac{1}{\lambda_e} + \frac{1}{d} \right)^{-1}, \quad (2)$$

where C_e is the electron volumetric heat capacity, v_f is the Fermi velocity, and λ_e is the electron MFP. We fit for the product of C_e and v_f , obtaining a thickness-dependent result for k_{TaN} .

Figures 3 and 4 report the results for $R_{\text{Al-TaN}}$ and k_{TaN} . Although the Al-TaN TBR decreases significantly after being heated, the heating and cooling curves for the TaN intrinsic thermal conductivity show no significant difference. This smooth temperature dependence of the thermal conductivity suggests that TaN is structurally stable up to 700 K. As Ono *et al.* demonstrated, a marked increase in the electrical resistance of a material accompanies increased species diffusion from the surrounding layers.¹³ This change is due to increased impurity density in the material of interest, which reduces electron MFP. Because electrons are a major thermal energy conductor in TaN, the structural failure of the film would similarly correspond to a substantial increase in thermal resistance. Given that the measurements show no

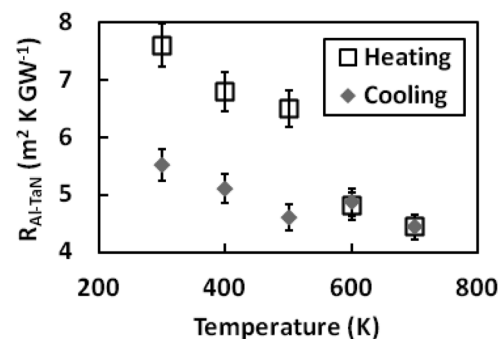


FIG. 3. Temperature-dependent Al-TaN TBR. The open squares represent the heating curve, and the closed diamonds represent the cooling curve. Note that $R_{\text{Al-TaN}}$ drops after heating above 600 K, demonstrating an improvement in interface quality.

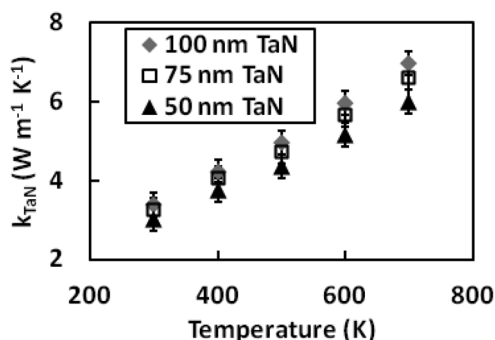


FIG. 4. Temperature-dependent intrinsic out-of-plane thermal conductivity of TaN for the 50-100 nm samples.

significant drop in out-of-plane k_{TaN} , it can be assumed that the TaN layer is structurally stable up to 700 K. Further, it is doubtful that the hysteresis shown in Fig. 3 is due to species diffusion between Al and TaN, as this typically increases TBR due to the presence of a disordered material layer.¹⁴ Rather, the results imply that interface annealing may reduce the dislocation density between the two films, lowering the interfacial carrier scattering rate.

At 300 K, the measured intrinsic thermal conductivity of TaN ranges from 3.0 to 3.4 $\text{W m}^{-1} \text{K}^{-1}$ for the 50-100 nm samples, lower than predicted from the Wiedemann-Franz-Lorenz law and minimum thermal conductivity theory. This is likely due to the earlier assumptions of isotropic electron conduction. Lateral electron conduction is less susceptible to boundary scattering than cross-plane conduction. As a result,

the theoretical prediction of cross-plane conductivity gives a larger result than observed. This disparity decreases for thicker TaN films. To account for this, a more rigorous theoretical treatment including both electron and phonon conduction is necessary. This suggests a Boltzmann Transport approach, which may be excessive in terms of constructing thermal models for systems containing TaN. For the purposes of creating such models, the data presented in this paper accurately represent the thermal behavior of these films.

This research was made with Government support under and awarded by DoD, Air Force Office of Scientific Research, National Defense Science and Engineering Graduate (NDSEG) Fellowship, 32 CFR 168a.

¹S. M. Rossmagel, *J. Vacuum Sci. Technol. B* **20**, 2328 (2002).

²M. Wittmer, *Appl. Phys. Lett.* **36**, 456 (1980).

³J. M. Daughton, *Thin Solid Films* **216**, 162 (1992).

⁴M. A. Panzer, M. Shandalov, J. A. Rowlette, Y. Oshima, C. Yi Wei, P. C. McIntyre, and K. E. Goodson, *IEEE Electron Device Lett.* **30**, 1269 (2009).

⁵K. Ujihara, *J. Appl. Phys.* **43**, 2376 (1972).

⁶E. H. Sondheimer, *Adv. Phys.* **1**, 1 (1952).

⁷E. Zhao, B. Hong, J. Meng, and Z. Wu, *J. Comput. Chem.* **30**, 2358 (2009).

⁸S. Tsukimoto, M. Moriyama, and M. Murakami, *Thin Solid Films* **460**, 222 (2004).

⁹G. A. Slack, *Solid State Physics* (Academic, New York, 1979), Vol. 34.

¹⁰J. Bryner, D. M. Profunser, J. Vollmann, E. Mueller, and J. Dual, *Ultrasonics* **44**, e1269 (2006).

¹¹A. Feldman, *High Temp. - High Press.* **31**, 293 (1999).

¹²D. G. Cahill, *Rev. Sci. Instrum.* **75**, 5119 (2004).

¹³H. Ono, T. Nakano, and T. Ohta, *Appl. Phys. Lett.* **64**, 1511 (1993).

¹⁴T. Beechem and P. E. Hopkins, *J. Appl. Phys.* **106**, 124301 (2009).